

Condition assessment of bridge pier using constrained minimum variance unbiased estimator

Pranjal Tamuly, Arunasis Chakraborty* and Sandip Das

Department of Civil Engineering, Indian Institute of Technology Guwahati, Assam, India- 781039

(Received April 17, 2020, Revised August 20, 2020, Accepted September 25, 2020)

Abstract. Inverse analysis of non-linear reinforced concrete bridge pier using recursive Gaussian filtering for in-situ condition assessment is the main theme of this work. For this purpose, minimum variance unbiased estimation using unscented sigma points is adopted here. The uniqueness of this inverse analysis lies in its approach for strain based updating of engineering demand parameters, where appropriate bound and constrained conditions are introduced to ensure numerical stability and convergence. In this analysis, seismic input is also identified, which is an added advantage for the structures having no dedicated sensors for earthquake measurement. First, the proposed strategy is tested with a simulated example whose hysteretic properties are obtained from the slow-cyclic test of a frame to investigate its efficiency and accuracy. Finally, the experimental test data of a full-scale bridge pier is used to study its in-situ condition in terms of Park & Ang damage index. Overall the study shows the ability of the augmented minimum variance unbiased estimation based recursive time-marching algorithm for non-linear system identification with the aim to estimate the engineering damage parameters that are the fundamental information necessary for any future decision making for retrofitting/rehabilitation.

Keywords: bouc-wen hysteresis; minimum variance unbiased estimation; condition assessment of bridge pier; shake table test; Park & Ang damage index

1. Introduction

Damage estimation of any structure after a catastrophic event such as earthquake is one of the primary concerns for civil engineers to ensure safety and serviceability. A common practice in this context is to estimate the damage by measuring the changes in modal frequencies and damping characteristics before and after the event. Several techniques are reported in the literature for determining the modal characteristics from the response. In time domain, eigen-system realization algorithm performs excellent for modal parameter identification of actual structures Qu *et al.* (2017). On the other hand, frequency decomposition techniques are also efficient in identifying the modal parameters even for closely spaced modes Qu *et al.* (2018a). In these problems, higher order spectrum provides a good measure to nullify the effects of random noise Qu *et al.* (2018b). Even attempt has been made to combine the time and frequency domain methods for better efficiency e.g. eigen-system realization algorithm and frequency response function are combined to identify the

*Corresponding author, Associate Professor, E-mail: arunasis@iitg.ac.in

model parameters of a bridge Qu *et al.* (2019). Further, the recent advancement in blind source separation techniques have shown promising ability to extract the modal information Yi *et al.* (2019). However, in case of reinforced concrete (RC) structure, the above procedure may not provide satisfactory result as they are designed to undergo inelastic deformation during an earthquake [Gaviria and Montejo (2019)]. Therefore, the severity of damage is underestimated, when it is quantified in terms of change in natural frequencies and damping Todorovska and Trifunac (2007), Hernandez and May (2012). Thus, damage estimation based on engineering demand parameters (EDP) such as peak displacement, inter-storey drift, hysteretic energy provides robust insight into the level of deterioration induced in it. Further, EDP based damage estimation provides a strong scientific basis for decision making to improve the structural performance against seismic risk and serve as a foundation for performance-based earthquake engineering in both design and post event maintenance. Among different EDPs, cumulative hysteretic energy-based damage quantification provides better estimation than other instantaneous parameters such as peak roof displacement and peak inter storey displacement Zahrah and Hall (1984), Ghosh *et al.* (2011). In this context, approximate methods are available in the literature to obtain the seismic demand of inelastic structures, where it is converted into an equivalent single degree of freedom (SDOF) system Li *et al.* (2016).

This non-linear hysteretic behaviour of RC structures under moderate to severe ground excitation imposes huge inelastic demand and is often manifested in cracking of concrete and yielding of reinforcement. The relationship between the restoring force and the output state variable in such structures is memory based i.e. the output not only depends upon the instantaneous state but also on its past history. Due to this reason, modelling the hysteretic behaviour of RC structure offers serious challenges. Besides modelling, measuring the restoring force acting in an actual system using instrumentation is also a daunting task. In the absence of measured restoring force, engineers often use the total inertia force acting on the structure under base excitation as the restoring force Gaviria and Montejo (2019), Shan *et al.* (2019). This is incorrect, since the contribution from inherent damping of the structure is not decoupled. Thus, the estimation of the actual restoring force of a real-life structural system has a growing appeal to the research community. To address this issue, several parametric identification techniques have been demonstrated in the literature Chang *et al.* (2016). Among them, recursive Kalman filter-based estimations are preferred by the researcher as they can utilize the available information (i.e., measurements) more efficiently. In these techniques, measurements are used to update the numerical model of the structure. Wu and Smyth (2007) have compared the performance of Extended Kalman filter (EKF) and Unscented Kalman filter (UKF) to identify the parameters of Bouc-Wen hysteretic SDOF structure and found that UKF offered a better estimation. Similarly, Song and Dyke (2013) have estimated the parameters of the modified Bouc-Wen model from the experimental response of a scaled (1/10) single storey shear building frame subjected to base excitation. Recently, Calabrese *et al.* (2018) have used constrained UKF algorithm, where sigma points are controlled during the updating process to restrict them within the parameter boundaries. It is shown that their proposal offered better results than the original UKF algorithm with the help of experimental response of a base isolated prototype structure. A different approach than the traditional UKF based identification technique has been developed by Bisht and Singh (2014), where they have adjusted the covariance matrix so that it can track any sudden change in stiffness. Zhang *et al.* (2016) have proposed improved EKF with Tikhonov regularization to identify the damage of a seven storied structure.

Besides time domain techniques, several other approaches are available in the literature for damage assessment of concrete structures. One of the commonly used technique is based on

acoustics emission, where deterioration in concrete is analyzed to trace the process of failure progression Nair *et al.* (2014). For rapid assessment, nondestructive evaluation techniques are commonly used, which are based on electrical resistivity (ER), impact echo (IE), ground-penetrating radar (GPR), and ultrasonic surface waves (USW) method Gucunski *et al.* (2015). Nowadays, cost effective Lead Zirconated Titanite (PZT) transducers are extensively used for damage detection of concrete structure. In this context, Tzoura *et al.* (2015) have utilized PZT sensors to measure the extent of damage in a concrete column for retrofitting. They have found that the electro-mechanical impedance provides more insight into the damage incurred in the structure. Providakis *et al.* (2015) have utilized this concept to investigate the damage in a concrete beam specimen. Wei *et al.* (2015) have monitored the corrosion of steel bar in a reinforced concrete beam by measuring the galvanic current flowing through it and have found that local stress level plays an important role on the extent of corrosion damage. Another study by Lin *et al.* (2017) shows the utilization of inexpensive strain gauges for damage detection of concrete arch bridges using virtual distortion method. The studies clearly demonstrate the necessity behind condition assessment of reinforced concrete structures. Although these non-destructive tests provide useful information about damage, they are not sufficient enough to characterize the phenomenological behaviour, which is essential for deciding appropriate rehabilitation work. The literature review presented above is mainly focused on two aspects - (i) time domain recursive identification of hysteretic systems and (ii) damage mechanism with its quantification in analysis and design of the reinforced concrete structure. In this context, it can be observed that Kalman filter or its advanced versions for system identification are well developed. Multiple researchers have extensively studied this inverse parameter identification strategy and have proposed different modifications to make their algorithm robust. Their studies are mainly focused on the filtering aspect involving different support point generation schemes or other regularization techniques for variance reduction of the error covariance matrix. Most of these studies are validated with simulation based synthetic experiments or small-scale laboratory tests in a controlled environment. However, these variants of Kalman filters have greater potential for parametric identification of non-linear behaviour often encountered in actual full-scale structure. One such example is the reinforced concrete structures that undergo inelastic deformation during seismic events. Thus, accurate estimation of model parameters defining the inelastic behaviour is a precondition for any reasonable retrofitting measure. This aspect of system identification in the light of Gaussian filtering is less represented in the literature. Besides inelastic parametric identification, estimation of input excitation is equally important as it helps to cross verify the designed demand of the original structure. In this paper, a comprehensive application of minimum variance unbiased estimator is carried out with a major focus towards damage estimation of reinforced concrete structure. The parameters obtained through this algorithm are subsequently used to estimate the restoring force acting on the structure which is not possible otherwise. Also, the identified hysteretic energy is utilized for the estimation of engineering damage parameters, which represent the accumulated damage. Hence, this paper aims to estimate the damage state of the reinforced concrete structure by utilizing recorded response with the help of minimum variance unbiased estimation. With these in view, the objectives of the present work are as follows –

1. Adopt constrained minimum variance unbiased estimator for parametric identification of Bouc-Wen hysteresis with degradation and pinching. For this purpose, design appropriate constraints for the bounded input and bounded output systems.

2. Validate the identified hysteretic energy and subsequent damage estimation using synthetic experiments. Modified Park & Ang damage index is proposed to be adopted as it is popular among the structural engineers.
3. Demonstrate the performance of the algorithm using shake table measurements of a full-scale inelastic response of a bridge pier. Quantify the input motion and damage index from the identified hysteretic energy, which can serve as the basis for decision making.

2. Phenomenological model of hysteresis

Modelling microscopic behaviour of any material and integrating them into macroscopic structural analysis is a difficult task. Although different material models are available in the literature Chang and Mander (1994), Ibarra *et al.* (2005) for calibration, problem is more complex for heterogeneous material like concrete. To alleviate this problem, phenomenological models are used extensively by the researchers and engineers for structural analysis. It consists of mathematical forms mainly focused on capturing macroscopic input-output relationships of the system. An extensive review of such models for RC structure is available in Sengupta and Li (2017). Among them, Bouc-Wen (1967) model has gained popularity because of its ability to demonstrate load vs deformation behaviour and produce hysteretic loops of different shapes and sizes. To apply this model, its parameters are tuned properly to match the experimental behaviour. Although, these phenomenological parameters are scalar quantities, identification algorithm for inverse problem needs specific bounds to maintain stability during numerical iterations using measurements Chatzi *et al.* (2010). To address this issue further, Ikhouane and Rodellar (2005) have proposed bounded input and bounded output (BIBO) property for the Bouc-Wen hysteretic model, which is essential for macroscopic analysis of structural and mechanical systems. This property indicates that the hysteretic system is defined to be BIBO, if every bounded input to the system results in a bounded output over the time interval. In this process, the system also dissipates energy when exposed to the external loading cycle. Let us assume a hysteretic system of the form Wen (1976)

$$F_r(x, z, t) = \alpha kx(t) + (1 - \alpha)kz(t) \quad (1a)$$

$$\dot{z}(t) = A\dot{x} - \beta|\dot{x}||z|^{n-1}z - \gamma\dot{x}|z|^n \quad (1b)$$

In the above equation, $\alpha \in (0,1)$ is the ratio of the post to pre-yield stiffness. $F_r(x, z, t)$ and $x(t)$ denote the restoring force and displacement of the hysteretic system, respectively, while $z(t)$ represents the non-observable hysteretic displacement, where overdot corresponds to the derivative with respect to time. The parameters which control the shape and size are denoted by $\{A, \beta, \gamma, n\}$ in the above equation. BIBO properties can be classified as shown in Table 1.

In this table z_0 and z_1 are the two constant defined as $z_0 \triangleq \frac{n\sqrt{A}}{\beta+\gamma}$ and $z_1 \triangleq \frac{n\sqrt{A}}{\gamma-\beta}$. Any other Bouc-

Wen model apart from these two classes does not represent hysteretic behaviour of a physical system Ikhouane and Rodellar (2005). It is hereditary in nature and hence, nonlinear Bayesian state estimation is difficult to solve without any prior knowledge. Thus, researchers have adopted suboptimal approaches to incorporate the behaviour of the systems in the form of constraints. One of the popular methods for this purpose is unscented recursive nonlinear dynamic data reconciliation (URNDDR) Mandela *et al.* (2012), Calabrese *et al.* (2018), where equality/inequality constraints are incorporated within the sigma points based

Table 1 Classification of Bouc-Wen model

Case		$\Omega_{A,\beta,\gamma,n}$	Upper bound on $ z(t) $	Class
$A > 0$	$\beta + \gamma > 0$ and $\beta - \gamma \geq 0$	R	$\max(z(0) , z_0)$	I
	$\beta + \gamma < 0$ and $\beta \geq 0$	$[-z_1, z_1]$	$\max(z(0) , z_0)$	II

predictor-corrector framework. In this framework, the sigma points lying outside the constraint region are forcefully brought back to its domain by projecting it on the boundary. However, this approach for constraint implementation can destroy the symmetry of the sigma points. Yang and Ma (2003) have developed constraint implementation for the nonlinear Bayesian state and parameter estimation, where the states corresponding to the system parameters are replaced by a continuous function, whose values lie between the assigned bounds. This idea is further modified by the authors of this paper for unscented sigma points based Bayesian estimation. In this method, the constrained conditions are imposed on the sigma points by treating them as a function of the auxiliary variables. To explain this, consider a state-space model with state X_1 and parameter θ as follows

$$\begin{bmatrix} \dot{X}_1 \\ \dot{\theta} \end{bmatrix} = \begin{bmatrix} f(X_1, \theta) \\ 0 \end{bmatrix} \tag{2}$$

Here, the parameter θ is bounded between $[l_1, l_2]$. In general, traditional Kalman-Filter cannot take into account bounds and algebraic constraints on system variables Kandepu *et al.* (2008). However, in this study, the authors have provided a unique improvisation for such problem. For this purpose, an auxiliary function $[c(X_2)]$ is introduced which lies within the bounds i.e. $l_1 \leq c(X_2) \leq l_2$ while the original state remains unbounded i.e., $-\infty < X_2 < \infty$. Thus, Eq. (2) can be expressed in the following form

$$\begin{bmatrix} \dot{X}_1 \\ \dot{X}_2 \end{bmatrix} = \begin{bmatrix} f(X_1, c(X_2)) \\ 0 \end{bmatrix} \tag{3}$$

A sinusoidal function is a good candidate to define bounds which is used in this paper. For example, parameter θ in the above state-space equation is expressed as a function of X_2 such that

$$\theta = l_1 \cos^2 X_2 + l_2 \sin^2 X_2 \tag{4}$$

Now, to characterize the hysteretic behaviour of the structural system, its BIBO property is ensured within the identification algorithm. Among the two classes of BIBO system in Table 1, only class I is stable and conforms with the real systems. Also, it can describe the property related to the hysteretic energy dissipation and is compatible with the laws of Thermodynamics Ikhouane *et al.* (2007). Hence, only BIBO class I property is considered in this study. This property is ensured by implicitly defining β and γ as a function two auxiliary variable X_β and X_γ , as given in the following expression

$$\beta = X_\beta^2 + X_\gamma^2 \tag{5a}$$

$$\gamma = X_\beta^2 - X_\gamma^2 \tag{5b}$$

Since, both β and γ are non-dimensional parameters, a quadratic function of auxiliary variables should not affect the consistency of the system equation. The verification of this claim regarding BIBO class I property

by Eq. (5) can be established by simple addition and subtraction of the two equations. Together Eqs. (4) and (5) provide stability to the estimator by confining the generation of sigma points within the predefined domain.

Though, there is a possibility of occurrence of optima outside this domain, however, such occurrence is very unlikely in case of realistic bounds as shown by Yang and Ma (2003).

2.1 Generalized Bouc-Wen model for RC structure

Although, Bouc-Wen model described in Eq. (1) can characterize different hysteretic load vs deformation behaviour, it is not sufficient to model similar behaviour of concrete. This is due to the reason that degradation and pinching are commonly observed in RC structure during extreme loading conditions. For this purpose, the Bouc-Wen-Baber-Noori (BWBN) hysteretic model is developed in the literature Baber and Noori (1985). The expression of the restoring force for BWBN system is provided by Eq. (1(a)) while Eq. (1(b)) is modified by relating the hysteretic displacement $z(t)$ with the total displacement $x(t)$ using the following expression

$$\dot{z}(t) = h(t) \frac{A\dot{x}(t) - \nu(t)(\beta|\dot{x}(t)||z(t)|^{n-1}z(t) + \gamma\dot{x}(t)|z(t)|^n)}{\eta(t)} \quad (6)$$

The dimensionless parameters A , β , γ and n in Eq. (6) are responsible for the fundamental shape of the hysteresis loop. Parameter A has a nominal effect on the overall hysteresis and hence, it is taken as unity in most of the cases Sengupta and Li (2013)] Three major modifications are introduced in Eq. (6) (viz. strength degradation, stiffness degradation and pinching effects), which are defined by the functions $\nu(t)$, $\eta(t)$ and $h(t)$, respectively. In general, strength and stiffness degradation depend on the duration and severity of the excitation which can be quantified in terms of cumulative hysteretic energy by the following expression

$$\varepsilon(t) = \int_0^t z\dot{x}dt \quad (7)$$

Here, it may be noted that functions $\nu(t)$ and $\eta(t)$ are proportional to $\varepsilon(t)$ which can be expressed by

$$\nu(t) = 1 + \delta_\nu \varepsilon(t) \quad (8a)$$

$$\eta(t) = 1 + \delta_\eta \varepsilon(t) \quad (8b)$$

where, δ_ν and δ_η are the constants responsible for the rate of strength and stiffness degradation, respectively. Finally, the pinching phenomenon is added by the function $h(t)$ which is given by

$$h(t) = 1 - \zeta_1(t) \exp\left(-\frac{(z(t)\text{sign}(\dot{x}(t)) - qz_u)^2}{(\zeta_2(t))^2}\right) \quad (9)$$

In the above equation, $\text{sign}(\cdot)$ represents the signum function and z_u is the ultimate value of $z(t)$ which is given by

$$z_u = \sqrt[n]{\frac{1}{\nu(t)(\beta + \gamma)}} \quad (10)$$

Functions $\zeta_1(t)$ and $\zeta_2(t)$ in Eq. (9) control pinching behaviour which are expressed as

$$\zeta_1(t) = (1 - e^{-p\varepsilon(t)})\zeta_0 \quad (11a)$$

$$\zeta_2(t) = (\psi_0 + \delta_\psi \varepsilon(t))(\lambda + \zeta_1(t)) \quad (11b)$$

In the above two equations, p determines the slope of the initial drop in the pinching region while ζ_0 , ψ , δ_ψ and λ control the rate and amount of pinching in the hysteresis loops. By optimizing these parameters, the actual hysteretic behavior of a RC structures can be modelled.

3. Constrained minimum variance unbiased estimation

The generalized minimum variance unbiased estimator (GMVU) has been developed by Song (2018) to estimate the state and input based on the sequential measurements with the help of unscented transformed points. In this paper, original GMVU algorithm is augmented with the constraint conditions to improve its performance and avoid instability associated with the identification of hysteretic system. The constrained minimum variance unbiased estimation algorithm is explained with the help of an n degree of freedom (DOF) nonlinear dynamic system, whose equation of motion can be expressed as

$$\mathbf{M}\ddot{\mathbf{x}}(t) + \mathbf{F}[\mathbf{x}(t), \dot{\mathbf{x}}(t), \Phi] = \mathbf{B}\mathbf{u}(t) + \mathbf{H}\mathbf{f}(t) \quad (12)$$

In the above equation, $\mathbf{x}(t)_{n \times 1} \in \mathbb{R}^n$, $\dot{\mathbf{x}}(t)_{n \times 1} \in \mathbb{R}^n$ and $\ddot{\mathbf{x}}(t)_{n \times 1} \in \mathbb{R}^n$ are the displacement, velocity and acceleration vector of the structure, respectively. The unknown parameter vector $\Phi_{m \times 1} \in \mathbb{R}^m$ has damping, stiffness and other nonlinear hysteretic parameters. Generally, the mass of the structure remains unaffected by damage during its life span and hence, the mass matrix \mathbf{M} is considered to be known, which can be easily computed from the material and geometric properties. $\mathbf{F}[\mathbf{x}(t), \dot{\mathbf{x}}(t), \Phi]$ represents the restoring force of the structure which is a function of displacement, velocity and other hysteretic model parameters. Further, $\mathbf{u}(t) \in \mathbb{R}^p$ and $\mathbf{f}(t) \in \mathbb{R}^q$ denote the known and unknown external forces, respectively while \mathbf{B} and \mathbf{H} represent the corresponding influence matrices. The extended state vector formed for the identification purpose can be expressed as

$$\mathbf{Z}(t) = \{\mathbf{Z}_1 \ \mathbf{Z}_2 \ \mathbf{Z}_3\}^T \quad (13)$$

where, $\mathbf{Z}_1 = \mathbf{x}(t)^T$; $\mathbf{Z}_2 = \dot{\mathbf{x}}(t)^T$ and $\mathbf{Z}_3 = \Phi^T$. The extended state vector in Eq. (13) is classified into two parts - time-dependent state vector, i.e. $\{\mathbf{Z}_1 \ \mathbf{Z}_2\}^T$ and time-invariant parameter vector i.e., $\dot{\mathbf{Z}}_3 = \dot{\Phi}^T = \mathbf{0}$. Using Eq. (13) in Eq. (12), the equation of motion can be expressed in state-space as

$$\begin{Bmatrix} \dot{\mathbf{Z}}_1^T \\ \dot{\mathbf{Z}}_2^T \\ \dot{\mathbf{Z}}_3^T \end{Bmatrix}_{(2n+m) \times 1} = \begin{Bmatrix} \mathbf{Z}_2^T \\ \mathbf{M}^{-1} \{ \mathbf{B}\mathbf{u}(t) + \mathbf{H}\mathbf{f}(t) - \mathbf{F}[\mathbf{Z}_1^T(t), \mathbf{Z}_2^T(t), \mathbf{Z}_3^T(t)] \} \\ \mathbf{0}_{m \times 1} \end{Bmatrix} \quad (14)$$

Therefore, the above equation can be represented in the general form of the non-linear differential state equation in continuous time as

$$\dot{\mathbf{Z}}(t) = \mathbf{G}(\mathbf{Z}(t), \mathbf{u}(t), \mathbf{f}(t)) \quad (15)$$

To implement the identification algorithm using real-time measurements, the system equation (i.e., Eq. (15)) is discretized in time domain as follows

$$\mathbf{Z}_k = \mathbf{Z}_{k-1} + \int_{(k-1)\Delta t}^{k\Delta t} [\mathbf{G}(\mathbf{Z}(t), \mathbf{u}(t), \mathbf{f}(t))] dt = \mathbf{g}(\mathbf{Z}_{k-1}, \mathbf{u}_{k-1}, \mathbf{f}_{k-1}) \quad (16)$$

The nonlinear measurement equation at any time $t = k\Delta t$ can be expressed by

$$\mathbf{y}_k = \mathbf{h}(\mathbf{Z}_k, \mathbf{u}_k) + \mathbf{H}_k \mathbf{f}_k + \mathbf{v}_k \quad (17)$$

In Eqs. (16) and (17), the state vector, known input vector and unknown input vector at $t = k\Delta t$ are denoted by \mathbf{Z}_k , \mathbf{u}_k and \mathbf{f}_k , respectively with sampling period Δt . The random measurement noise \mathbf{v}_k is considered to be zero mean Gaussian with covariance $\mathbb{E}[\mathbf{v}_i \mathbf{v}_j^T] = \mathbf{R}_{ij} \delta_{ij}$, where δ_{ij} is the Kronecker delta. The feedthrough coefficient matrix $\mathbf{H}_k = \mathbf{H}(k\Delta t) \in \mathbb{R}^{q \times p}$ has full column rank i.e., $\text{rank}(\mathbf{H}_k) = p$.

In this study, the nonlinear hysteretic system is characterized with the help of Bouc-Wen hysteretic model. With this in view, the extended state vector related to the Bouc-Wen hysteretic system is expressed as

$$\mathbf{Z}_k = \{\mathbf{A}_k \quad \mathbf{\Phi}_k\}^T \quad (18)$$

where, vector $\mathbf{A}_k = \{\mathbf{x}_k \quad \dot{\mathbf{x}}_k\}$ denotes the displacement and velocity, respectively while the vector $\mathbf{\Phi}_k$ represents the unknown parameters of the Bouc-Wen model. To improve the performance of the identification schemes, prior knowledge of the Bouc-Wen system is incorporated in the estimation algorithm as constrained conditions which is explained in Section 2. For this purpose, the unknown parameter vector $\mathbf{\Phi}_k$ is augmented with other unknown parameters as $\mathbf{\Phi}_k = \{\mathbf{\Theta} \quad \beta \quad \gamma \quad \mathbf{w}\}$ where, $\mathbf{\Theta} = \{\theta_1 \quad \theta_2 \quad \theta_3 \dots \theta_n\}$ has the parameters with bounds, \mathbf{w} denotes the parameter vector without any bounds, while β and γ are the Bouc-Wen parameters related to BIBO properties. In this study, \mathbf{w} consists of stiffness and damping coefficients while vector $\mathbf{\Theta}$ consists of the Bouc-Wen model parameters other than β and γ . Next, the upper and lower bounds of parameters belonging to $\mathbf{\Theta}$ are provided with the help of Eq. (4) and similarly, the BIBO properties are ascertained using Eq. (5).

The minimum variance unbiased estimator algorithm helps to quantify both system state \mathbf{Z}_k and external unknown input force \mathbf{f}_k based on the sequential measurements $\{\mathbf{y}_1, \mathbf{y}_2, \dots, \mathbf{y}_k\}$. The estimate of state \mathbf{Z}_k and unknown force \mathbf{f}_k at any time instant k is denoted as $\tilde{\mathbf{Z}}_{0|k}^T$ and $\tilde{\mathbf{f}}_0^T$, respectively. For initialization, i.e., at $t = 0$, the unbiased estimate of initial state \mathbf{Z}_0 is assumed to be $\tilde{\mathbf{Z}}_{0|0}$ and the same for \mathbf{f}_0 is assumed to be $\tilde{\mathbf{f}}_0^T$. Similarly, the corresponding variance matrices $\mathbf{P}_{0|0}^Z$, \mathbf{P}_0^f and the cross-covariance matrices \mathbf{P}_0^{Zf} are considered to be known in this step. To estimate \mathbf{Z}_k and \mathbf{f}_k simultaneously, an augmented state vector \mathbf{X}_0 is formed whose initial estimate $\tilde{\mathbf{X}}_{0|0}$ and corresponding covariance matrix $\mathbf{P}_{0|0}^X$ can be expressed as follows

$$\tilde{\mathbf{X}}_{0|0} = [\tilde{\mathbf{Z}}_{0|0}^T \quad \tilde{\mathbf{f}}_0^T]^T \quad (19)$$

$$\mathbf{P}_{0|0}^X = \mathbb{E}[(\mathbf{X}_0 - \tilde{\mathbf{X}}_{0|0})(\mathbf{X}_0 - \tilde{\mathbf{X}}_{0|0})^T] = \begin{bmatrix} \mathbf{P}_{0|0}^Z & \mathbf{P}_0^{Zf} \\ (\mathbf{P}_0^{Zf})^T & \mathbf{P}_0^f \end{bmatrix} \quad (20)$$

In this study, both $\mathbf{g}(\cdot)$ and $\mathbf{h}(\cdot)$ in Eqs. (16) and (17) are nonlinear functions and hence, the evaluation of $\tilde{\mathbf{Z}}_{k|k-1}$, $\mathbf{P}_{k|k-1}^Z$ and $\mathbf{P}_{k|k-1}^{Zf}$ in statistical sense are very difficult. Here, it should be noted that the

subscript $(k|k-1)$ denotes the estimate of the same at time step k provided the measurements are available up to $(k-1)$ time step. To deal with this problem, Julier and Uhlmann (1997) proposed unscented transformation, where statistical moments are estimated with the help of deterministically chosen sampling points, known as unscented sigma points. Because of its accuracy and convenience, unscented sigma points based method is adopted here to propagate the system state through $\mathbf{g}(\cdot)$ and $\mathbf{h}(\cdot)$ functions. To implement this approach, at any time step k , $2n+1$ numbers (n is the total number of state) of unscented sigma points $\Psi_{k-1|k-1}$ are generated from the estimates of $\tilde{\mathbf{X}}_{k-1|k-1}$ and covariance $\mathbf{P}_{k-1|k-1}^{\mathbf{X}}$ using the following expression

$$\Psi_{k-1|k-1} = [\tilde{\mathbf{X}}_{k-1|k-1} \quad \tilde{\mathbf{X}}_{k-1|k-1} + \Gamma_i \quad \tilde{\mathbf{X}}_{k-1|k-1} - \Gamma_i] \tag{21}$$

In this equation, Γ_i is the i^{th} column of the matrix which has the form $\Gamma_i = \left\{ \sqrt{(n+\lambda)\mathbf{P}_{k-1|k-1}^{\mathbf{X}}} \right\}_i$. The scaling parameter λ is defined as $\lambda = \alpha^2(n+\kappa) - n$ and the spread of the sigma points are determined by the parameter α , which is normally set to a small positive value (i.e., $\alpha \leq 1$), while κ is a secondary scaling parameter usually set to 0 or $(3-n)$. The corresponding weights for the sample mean (\mathbf{W}^m) and covariance (\mathbf{W}^c) are given by

$$\mathbf{W}_1^m = \frac{\lambda}{n+\lambda} \tag{22a}$$

$$\mathbf{W}_1^c = \frac{\lambda}{n+\lambda} + (1 - \alpha^2 + \rho) \tag{22b}$$

$$\mathbf{W}_i^m = \mathbf{W}_i^c = \frac{1}{2(n+\lambda)} \quad i = 2, 3, \dots, 2n+1 \tag{22c}$$

For implementation, these sigma points are classified into two groups $(\Psi_{k-1|k-1}^z)^T$ and $(\Psi_{k-1|k-1}^f)^T$, corresponding to the system state and the unknown input, respectively i.e.

$$\Psi_{k-1|k-1} = \left[(\Psi_{k-1|k-1}^z)^T \quad (\Psi_{k-1|k-1}^f)^T \right]^T \tag{23}$$

These sigma points are transmitted through the nonlinear system equation [i.e. Eq. (16)] to get the predicted sigma points $\Psi_{k|k-1}$ as follows

$$\Psi_{k|k-1} = \mathbf{g}(\Psi_{k-1|k-1}^z, \mathbf{u}_{k-1}, \Psi_{k-1|k-1}^f) \tag{24}$$

This process also allows to estimate the statistical properties in terms of the system state $\tilde{\mathbf{Z}}_{k|k-1}$ and the covariance $\mathbf{P}_{k|k-1}^z$ as follows

$$\tilde{\mathbf{Z}}_{k|k-1} = \mathbb{E}[\mathbf{g}(\mathbf{Z}_{k-1}, \mathbf{u}_{k-1}, \mathbf{f}_{k-1})] \approx \sum_{i=1}^{2n+1} \mathbf{W}_i^m \Psi_{i,k|k-1}^z \tag{25a}$$

$$\begin{aligned} \mathbf{P}_{k|k-1}^z &= \mathbb{E} \left[(\mathbf{Z}_k - \tilde{\mathbf{Z}}_{k|k-1})(\mathbf{Z}_k - \tilde{\mathbf{Z}}_{k|k-1})^T \right] \\ &\approx \sum_{i=1}^{2n+1} \mathbf{W}_i^c (\Psi_{i,k|k-1}^z - \tilde{\mathbf{Z}}_{k|k-1})(\Psi_{i,k|k-1}^z - \tilde{\mathbf{Z}}_{k|k-1})^T \end{aligned} \tag{25b}$$

where, $\Psi_{i,k|k-1}^z$ denotes the i^{th} column of the matrix $\Psi_{k|k-1}^z$. Using the definition $\hat{\mathbf{y}}_k \triangleq \mathbf{y}_k - \mathbb{E}[\mathbf{h}(\mathbf{Z}_k, \mathbf{u}_k)]$, Eq. (17) can be expressed as follows

$$\hat{\mathbf{y}}_k = \mathbf{H}_k \mathbf{f}_k + \mathbf{e}_k \quad (26a)$$

In the above equation, the error \mathbf{e}_k is given by

$$\mathbf{e}_k \triangleq \mathbf{h}(\mathbf{Z}_k, \mathbf{u}_k) + \mathbf{v}_k - \mathbb{E}[\mathbf{h}(\mathbf{Z}_k, \mathbf{u}_k)] \quad (26b)$$

The statistical mean $\tilde{\boldsymbol{\Sigma}}_{k|k-1} = \mathbb{E}[\mathbf{h}(\mathbf{Z}_k, \mathbf{u}_k)]$ and the error covariance $\mathbf{P}_k^e = \mathbb{E}[\mathbf{e}_k \mathbf{e}_k^T]$ can be obtained from the predicted sigma points $\boldsymbol{\Psi}_{k|k-1}^Z$ as follows

$$\tilde{\boldsymbol{\Sigma}}_{k|k-1} \approx \sum_{i=1}^{2n+1} \mathbf{W}_i \boldsymbol{\Omega}_{i,k|k-1} \quad (27a)$$

$$\mathbf{P}_k^e \approx \sum_{i=1}^{2n+1} \mathbf{W}_i (\boldsymbol{\Omega}_{i,k|k-1} - \tilde{\boldsymbol{\Sigma}}_{k|k-1}) (\boldsymbol{\Omega}_{i,k|k-1} - \tilde{\boldsymbol{\Sigma}}_{k|k-1})^T + \mathbf{R}_k \quad (27b)$$

where, $\boldsymbol{\Omega}_{k|k-1} = \mathbf{h}(\boldsymbol{\Psi}_{k|k-1}^Z, \mathbf{u}_k)$ is the matrix representing the sigma points after transmitted through the nonlinear function $\mathbf{h}(\cdot)$ and \mathbf{R}_k denotes the covariance of the additive noise \mathbf{v}_k . Now, an estimate of the unknown input $\tilde{\mathbf{f}}_k$ can be obtained from $\hat{\mathbf{y}}_k$ in Eq. (26(a)) by using a scaling matrix \mathbf{C}_k as follows

$$\tilde{\mathbf{f}}_k = \mathbf{C}_k \hat{\mathbf{y}}_k = \mathbf{C}_k (\mathbf{H}_k \mathbf{f}_k + \mathbf{e}_k) \quad (28)$$

Taking expectation on both sides and using $\mathbb{E}(\mathbf{e}_k) = \mathbf{0}$ in Eq. (28) leads to

$$\mathbb{E}(\tilde{\mathbf{f}}_k) = \mathbf{C}_k \mathbf{H}_k \mathbb{E}(\mathbf{f}_k) \quad (29)$$

The above equation implies that $\tilde{\mathbf{f}}_k$ is an unbiased estimate, if and only if $\mathbf{C}_k \mathbf{H}_k = \mathbf{I}$, where, \mathbf{I} is the identity matrix. The assumption made previously that $\text{rank}(\mathbf{H}_k) = p$ is a necessary and sufficient condition for the existence of unbiased estimator in Eq. (29) Song (2018). Further, an optimal \mathbf{C}_k is also required for the minimum variance estimate of $\tilde{\mathbf{f}}_k$. For this purpose, it is assumed that \mathbf{P}_k^e is a positive definite matrix and there exists an invertible matrix \mathbf{Y}_k such that $\mathbf{Y}_k \mathbf{Y}_k^T = \mathbf{P}_k^e$. On pre-multiplying both sides of Eq. (26(a)) by \mathbf{Y}_k^{-1} , the following expression is obtained

$$\mathbf{Y}_k^{-1} \hat{\mathbf{y}}_k = \mathbf{Y}_k^{-1} \mathbf{H}_k \mathbf{f}_k + \mathbf{Y}_k^{-1} \mathbf{e}_k \quad (30)$$

Now, under the assumption that $\mathbf{Y}_k^{-1} \mathbf{H}_k$ is full column rank, the minimum variance estimation of $\tilde{\mathbf{f}}_k$ can be expressed from the above equation using Gauss-Markov theorem as Gillijns and De Moor (2007a)

$$\begin{aligned} \tilde{\mathbf{f}}_k &= \left[(\mathbf{Y}_k^{-1} \mathbf{H}_k)^T (\mathbf{Y}_k^{-1} \mathbf{H}_k) \right]^{-1} (\mathbf{Y}_k^{-1} \mathbf{H}_k)^T (\mathbf{Y}_k^{-1} \hat{\mathbf{y}}_k) \\ &= [\mathbf{H}_k^T (\mathbf{P}_k^e)^{-1} \mathbf{H}_k]^{-1} \mathbf{H}_k^T (\mathbf{P}_k^e)^{-1} \hat{\mathbf{y}}_k = \mathbf{C}_k \hat{\mathbf{y}}_k \end{aligned} \quad (31)$$

This optimal value of $\mathbf{C}_k = [\mathbf{H}_k^T (\mathbf{P}_k^e)^{-1} \mathbf{H}_k]^{-1} \mathbf{H}_k^T (\mathbf{P}_k^e)^{-1}$ from Eq. (31) and $\boldsymbol{\Omega}_{k|k-1}$ are used to obtain $\tilde{\mathbf{f}}_k$ as follows Song (2018)

$$\tilde{\mathbf{f}}_k = \mathbf{C}_k \tilde{\mathbf{y}}_k = \mathbf{C}_k \{ \mathbf{y}_k - \mathbb{E}[\mathbf{h}(\mathbf{Z}_k, \mathbf{u}_k)] \} \approx \mathbf{C}_k (\mathbf{y}_k - \sum_{i=1}^{2n+1} \mathbf{W}_i^m \boldsymbol{\Omega}_{i,k|k-1}) \quad (32)$$

From Eqs. (26(a)) and (31), the error in the estimated input $\tilde{\mathbf{f}}_k$ can be expressed as

$$\mathbf{f}_k^{er} = \mathbf{f}_k - \tilde{\mathbf{f}}_k = -\mathbf{C}_k \mathbf{e}_k \quad (33)$$

Additionally, the covariance \mathbf{P}_k^f related to the input error is obtained after substituting \mathbf{C}_k from Eq. (31) as follows

$$\mathbf{P}_k^f \triangleq \mathbb{E}[\mathbf{f}_k^{er} (\mathbf{f}_k^{er})^T] = \mathbf{C}_k \mathbf{P}_k^e \mathbf{C}_k^T = [\mathbf{H}_k^T (\mathbf{P}_k^e) \mathbf{H}_k]^{-1} \quad (34)$$

In the next step, the predicted estimates $\tilde{\mathbf{Z}}_{k|k-1}$ are updated to obtain new state $\tilde{\mathbf{Z}}_{k|k}$ with the help of available measurements \mathbf{y}_k as follows

$$\begin{aligned} \tilde{\mathbf{Z}}_{k|k} &= \tilde{\mathbf{Z}}_{k|k-1} + \mathbf{L}_k \{\mathbf{y}_k - \mathbb{E}[\mathbf{g}(\mathbf{Z}_k, \mathbf{u}_k)]\} \\ &\approx \sum_{i=1}^{2n+1} \mathbf{W}_i \boldsymbol{\Psi}_{i,k|k-1}^Z + \mathbf{L}_k (\mathbf{y}_k - \sum_{i=1}^{2n+1} \mathbf{W}_i \boldsymbol{\Psi}_{i,k|k-1}^Z) \end{aligned} \quad (35)$$

where, \mathbf{L}_k is the optimal gain matrix which yields minimum variance unbiased estimate of state \mathbf{Z}_k . The corresponding state estimation error $\tilde{\mathbf{Z}}_{k|k}^{er}$ can be expressed using Eqs. (26(a)) and (35) as follows

$$\tilde{\mathbf{Z}}_{k|k}^{er} \triangleq \mathbf{Z}_k - \tilde{\mathbf{Z}}_{k|k} = \tilde{\mathbf{Z}}_{k|k-1}^{er} - \mathbf{L}_k \mathbf{e}_k - \mathbf{L}_k \mathbf{H}_k \mathbf{f}_k \quad (36)$$

Applying expectation operator on both sides of Eq. (36) leads to $\mathbb{E}(\tilde{\mathbf{Z}}_{k|k}^{er}) = \mathbf{L}_k \mathbf{H}_k \mathbb{E}(\mathbf{f}_k)$, which suggests that $\tilde{\mathbf{Z}}_{k|k}$ is an unbiased estimation for all feasible value of \mathbf{f}_k , if and only if $\mathbf{L}_k \mathbf{H}_k = 0$. Assuming this unbiased condition is satisfied, the updated covariance $\mathbf{P}_{k|k}^Z$ associated with the state $\tilde{\mathbf{Z}}_{k|k}$ can be expressed using Eq. (36) as follows

$$\mathbf{P}_{k|k}^Z \triangleq \mathbb{E}[\tilde{\mathbf{Z}}_{k|k}^{er} (\tilde{\mathbf{Z}}_{k|k}^{er})^T] = \mathbf{P}_{k|k-1}^Z - \mathbf{L}_k \mathbf{P}_{k|k-1}^{Ze} - \mathbf{P}_{k|k-1}^{Ze} \mathbf{L}_k^T + \mathbf{L}_k \mathbf{P}_{k|k-1}^e \mathbf{L}_k^T \quad (37)$$

where, $\mathbf{P}_{k|k-1}^{Ze}$ is the corresponding cross covariance matrix having the following form

$$\begin{aligned} \mathbf{P}_{k|k-1}^{Ze} &\triangleq \mathbb{E}(\tilde{\mathbf{Z}}_{k|k-1}^{er} \mathbf{e}_k^T) = \mathbb{E}[\tilde{\mathbf{Z}}_{k|k-1}^{er} \{\mathbf{h}(\mathbf{Z}_k, \mathbf{u}_k) - \mathbb{E}[\mathbf{h}(\mathbf{Z}_k, \mathbf{u}_k)]\}^T] \\ &\approx \sum_{i=1}^{2n+1} \mathbf{W}_i^C (\boldsymbol{\Omega}_{i,k|k-1} - \tilde{\boldsymbol{\Xi}}_{k|k-1}) (\boldsymbol{\Psi}_{i,k|k-1}^Z - \tilde{\mathbf{Z}}_{k|k-1})^T \end{aligned} \quad (38)$$

To obtain the optimal gain matrix \mathbf{L}_k , the trace of $\mathbf{P}_{k|k}^Z$ is minimized under the constrained condition $\mathbf{L}_k \mathbf{H}_k = 0$. Based on the derivation provided by Gillijns and De Moor (2007b), its optimal value is given by

$$\mathbf{L}_k = \mathbf{K}_k (\mathbf{I} - \mathbf{H}_k \mathbf{C}_k) \quad (39)$$

In which, \mathbf{K}_k is similar to the Kalman gain matrix of the form

$$\mathbf{K}_k = \mathbf{P}_{k|k-1}^{Ze} (\mathbf{P}_k^e)^{-1} \quad (40)$$

Now, the updated covariance matrix $\mathbf{P}_{k|k}^Z$ can be obtained by substituting \mathbf{L}_k from Eq. (39) in Eq. (37) and rearranging them Song (2018) i.e.

$$\mathbf{P}_{k|k}^Z = \mathbf{P}_{k|k-1}^Z - \mathbf{K}_k (\mathbf{P}_k^e - \mathbf{H}_k \mathbf{P}_k^f \mathbf{H}_k^T) \mathbf{K}_k^T \quad (41)$$

Similarly, using Eq. (31), Eq. (33) and Eq. (36), the updated cross covariance matrix $\mathbf{P}_{k|k}^{Zf} \triangleq \mathbb{E}[\tilde{\mathbf{Z}}_{k|k}^{er} (\mathbf{f}_k^{er})^T]$ is obtained as Song (2018)

$$\mathbf{P}_k^{Zf} = -\mathbf{P}_{k|k-1}^{Ze} (\mathbf{C}_k)^T \quad (42)$$

For the next time step, the estimated states $\tilde{\mathbf{Z}}_{k|k}$, $\tilde{\mathbf{f}}_k$ and the corresponding covariance matrices $\mathbf{P}_{k|k}^Z$, \mathbf{P}_k^f and \mathbf{P}_k^{Zf} are substituted into Eqs. (19) and (20) and the iterative process continues. The flowchart of the proposed algorithm is shown in Fig. 1.

4. Damage quantification

In this study, major emphasis is given on in-situ condition assessment of RC structures using the above-mentioned algorithm. Damage quantification plays a vital role in any post-earthquake decision making procedures based on which appropriate measures are taken. This involves repair and/or strengthening of the structure as well as to predict the remaining service life of the structure. Damage quantification in terms of Damage index (DI) is more convenient to the designers because of its ability to state the damage level of the structure by a dimensionless number. In general, DI is a mathematical function based on some representative variables to quantify the damage of a structure or its components.

These representative variables are generally related to irrecoverable or inelastic deformations such as strains, curvatures, rotations, displacements and sometimes forces e.g. base shears, member resistances or energy dissipated during the inelastic reversed cyclic loading. Different types of DI have been reported in the literature for damage estimation of reinforced concrete structure Williams and Sexsmith (1995).

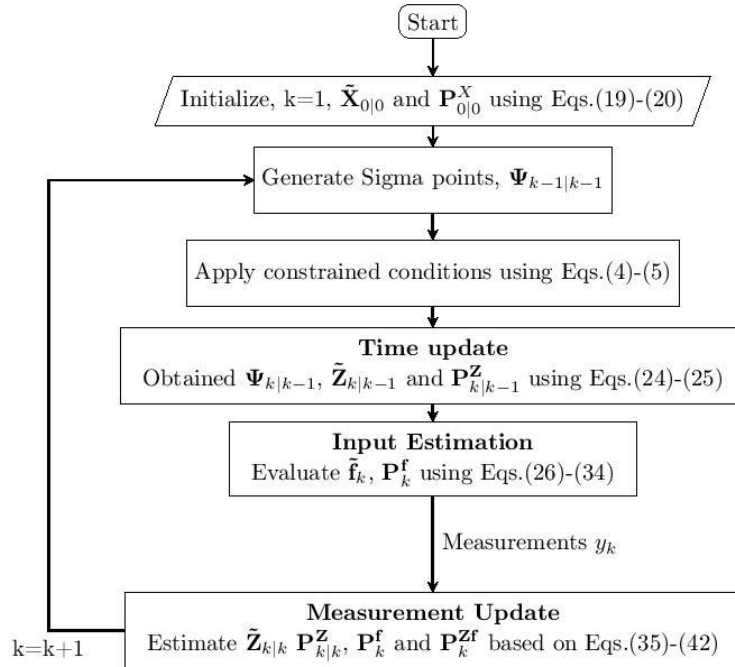


Fig. 1 Flowchart of the proposed constrained minimum variance unbiased estimation algorithm

Among them, the most widely used modified Park and Ang (1985) DI is selected here for its ability to provide best correlation with the laboratory results Ghosh *et al.* (2011). It has been accepted worldwide that the damage induced in a structural system during an earthquake not only depends on the maximum deformation but also on the hysteretic energy dissipated during the load cycles. The modified Park and Ang DI combines the above two aspects to provide a better characterization of the damage. In this model, both ductility demand and cumulative hysteretic energy demand are incorporated as a linear combination of normalized deformation and hysteretic energy adsorption, i.e.

$$DI = \frac{\delta_m - \delta_y}{\delta_u - \delta_y} + \beta_d \frac{\int dE_h}{F_y \delta_u} \quad (43)$$

where, δ_m , δ_u and δ_y are the maximum displacement, ultimate displacement and yield displacement, respectively and F_y is the yield force while $\int dE_h$ is the dissipated hysteresis energy in each the loading cycle. The nonzero positive parameter β_d refers to the strength degradation of the structural member. However, evaluation of the dissipated hysteresis energy is not straight forward since it cannot be obtained directly from the measurement itself. In practice, researchers used to obtain this from the updated finite element model such that the response generated by the model matches with the experiment within an acceptable range of accuracy. Although the forward problem is well-posed, the inverse problem to estimate them are difficult. In this paper, the hysteretic energy is estimated from the identified Bouc-Wen model using the above-mentioned algorithm. For this purpose, the measurements obtained from the system are provided to the constrained minimum variance unbiased estimator and the parameters related to hysteretic energy are estimated subsequently. The proposed algorithm is first validated using a synthetic experiment which is followed by the full-scale test of a bridge pier on shake table. These are discussed in the following section.

5. Numerical results and discussion

In this section, numerical results are presented to show the above-mentioned approach to estimate the extent of damage in a reinforced concrete structure when exposed to seismic ground motion. In this context, it may be noted that civil structures are designed by complying modern seismic codes to respond non-linearly during a seismic event. These structures experience degradation and pinching under extreme repetitive cyclic loading. With this in view, the present study aims to modify the already existing GMVU algorithm and adopt it to quantify the damage which is otherwise extremely difficult. First the algorithm is validated using a simulated example. It is followed by full scale testing of a bridge pier, which are explained in detail below.

5.1 Synthetic experiment for engineering demand parameter estimation

A 2-DOF structural system subjected to external ground motion where base columns are modelled by Bouc-Wen spring is considered to simulate the hysteretic response as shown in Fig. 2. Here, BWBN hysteretic model is used as explained in section 2.1 to simulate the actual behavior of the RC structure under extreme loading. The equation of motion for this system can be written as

$$m_1 \ddot{x}_1 + c_1 \dot{x}_1 + c_2 (\dot{x}_1 - \dot{x}_2) + \alpha k_1 x_1 + (1 - \alpha) k_1 z + k_2 (x_1 - x_2) = -m_1 \ddot{u}_g \quad (44a)$$

$$m_2 \ddot{x}_2 + c_2 (\dot{x}_2 - \dot{x}_1) + k_2 (x_2 - x_1) = -m_2 \ddot{u}_g \quad (44b)$$

where, non-observable hysteretic displacement $z(t)$ can be defined by Eq. (6). Eq. (8)-(11(b)) provide additional constitutive equations for this numerical model. Here, $m_1 = m_2 = 1120\text{kg}$, $k_1 = k_2 = 3.5 \times 10^6 \text{ N/m}$, $c_1 = c_2 = 6000\text{Ns/m}$ and BWBN model has the optimized parameters obtained from a pseudo static test data [Nithin (2019)] of a frame as shown in Fig. 3. The details of these parameters are given in Table 2. The measurements of this system are generated artificially by applying the ground motion at the base. In this analysis, the Imperial Valley 1940 ground motion record is used to generate the measurements (i.e., displacements and accelerations) using 4th order Runge-Kutta integration scheme. Here, it should be noted that the proposed algorithm has no pre-requisite for a particular seismic input and works for any recorded motion. Since the main objective of this study is the engineering damage parameter estimation, the input motion is selected in such a way that it can take the structure into its inelastic excursion. For this reason, the PGA, strong motion duration and frequency content of the signal are the most important parameters behind its selection. Thus, El-Centro motion is used in this example, which is widely used for non-linear analysis and design of structures. A zero-mean Gaussian white noise process with 2% RMS noise to signal ratio is added artificially. To apply the constraints as discussed in section 2, the extended state vector is formed (i.e., as in Eq. (18)), where, $\mathbf{\Lambda} = \{x_1 \ x_2 \ \dot{x}_1 \ \dot{x}_2 \ z\}$, $\mathbf{\Theta} = \{\alpha \ n \ \delta_v \ \delta_\eta \ p \ \zeta_0 \ \psi_0 \ \delta_\psi \ \lambda \ q\}$ and $\mathbf{w} = [k_1 \ k_2 \ c_1 \ c_2]$. The initial values of these parameters are assumed to be: $k_1 = k_2 = 2.5 \times 10^6 \text{ N/m}$, $c_1 = c_2 = 3000 \text{ Ns/m}$, $\alpha = 0.1$, $\beta = 0.04$, $\gamma = 0.03$, $\delta_v = 0.22$, $\delta_\eta = 0.01$, $p = 0.4$, $\zeta_0 = 0.80$, $\psi_0 = 0.58$, $\delta_\psi = 0.15$, $\lambda = 0.57$ and $q = 0.05$. The rationale behind the selection of these initial values are that they must be as realistic as possible. With an unfavourable guess, the algorithm may take longer time for convergence, which may not be feasible within the time window of the seismic input. The bounds related to parameter vector $\mathbf{\Theta}$ has been incorporated as constrained conditions using Eq. (4). Similarly, the BIBO properties are also maintained using Eq. (5). In this context, it should be noted that the prior to set the bounds, a brief design-of-experiment is carried out to check the effective range of the parameters to avoid any

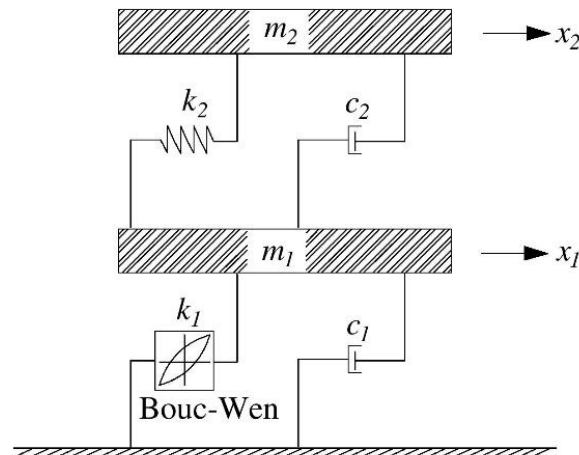


Fig. 2 Hysteretic structural system

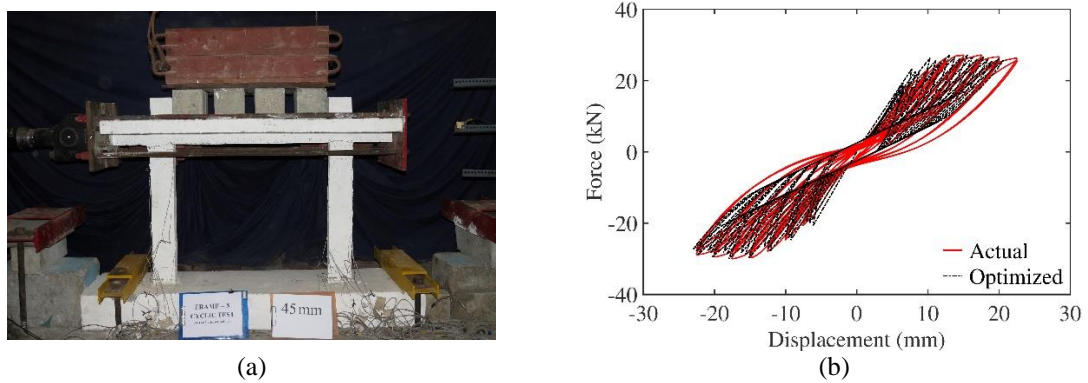


Fig. 3 Optimized BWBN hysteresis using slow cyclic test; (a) test setup & (b) actual and optimized hysteresis

numerical instability. These parameter bounds help to maintain convergence and stability to the algorithm. The value of these bounds in the numerical exercise are $0 \leq p \leq 5$; $1 \leq n \leq 6$. All other parameters from Θ are considered to be bounded between the interval $[0,1]$. The displacements and accelerations are used as the measurements in the identification algorithm i.e., $\mathbf{y} = [x_1 \ x_2 \ \ddot{x}_1 \ \ddot{x}_2]$. Fig. 4 shows the estimated stiffness and damping parameters. It can be clearly seen that both these parameters are successfully identified by the proposed algorithm with a high level of accuracy. Similarly, the Bouc-Wen parameters also converged to its true value as shown in Fig. 5(a). Bouc-Wen parameters, the algorithm can accurately identify the input ground motion as shown in Fig. 5(b). Thus, it can be concluded that the proposed algorithm can identify the non-linear hysteretic parameters as well as the input force of a reinforced concrete structure satisfactorily. However, the main focus of this study is the estimation of engineering damage

Table 2 BWBN parameters for validation exercise

Parameters	Optimized Parameter
α	0.1530370000
β	0.3001838000
γ	-0.2838606000
n	1.0003970000
δ_v	0.0047967490
δ_η	0.0000000588
p	2.7916030000
ζ_0	0.9265840000
ψ_0	0.1999966000
δ_ψ	0.0021046610
λ	0.9994293000
q	0.0000212757

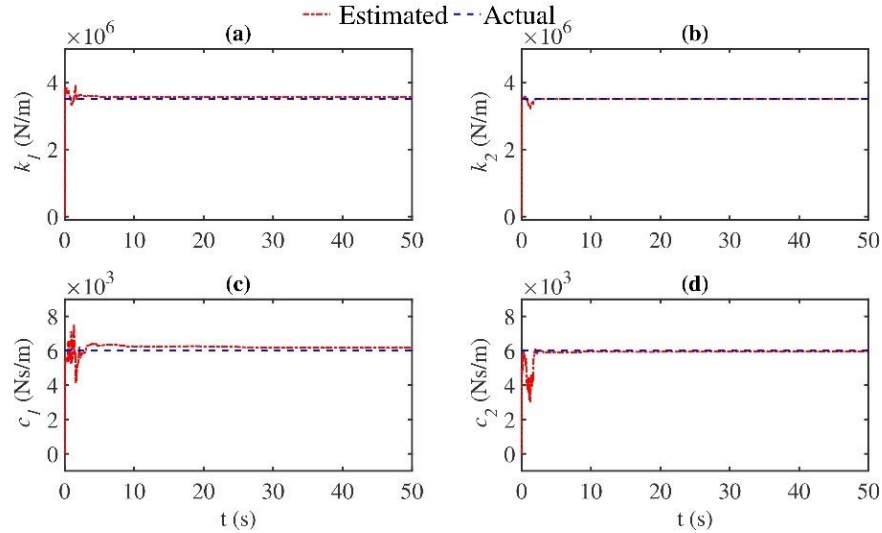


Fig. 4 Identified stiffness and damping parameters of 2-DOF system; (a) stiffness in storey 1, (b) in storey 2, (c) damping in storey 1 and (d) damping in storey 2

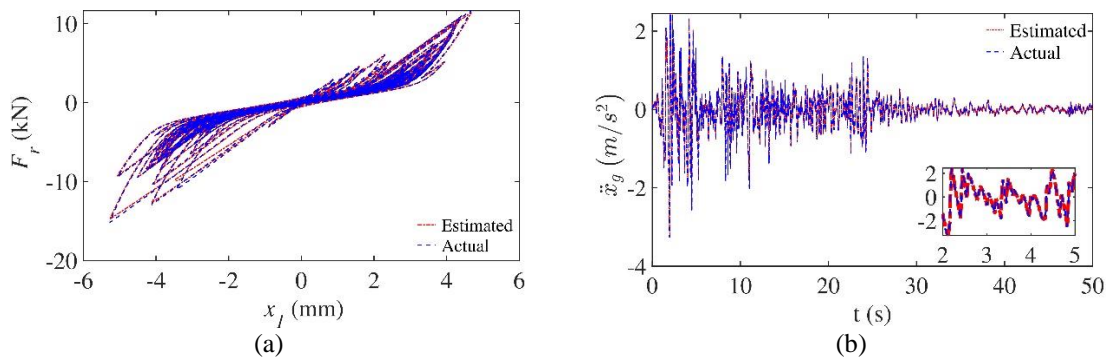


Fig. 5 Identified BWBN hysteresis and input; (a) load vs deflection and (b) seismic excitation

parameters using Park and Ang damage index i.e., maximum displacement (δ_m) and dissipated hysteretic energy ($\int dE_h$). In this estimation, the capacity related parameters such as ultimate displacement (δ_u) and yield force (F_y) remained unchanged. Hence, only the engineering damage parameters are responsible for the damage index value obtained after any seismic event. The comparison of estimated and actual engineering damage parameters is provided in Table 3 for 2% RMS noise. The small percentage error between the estimated and actual values of engineering damage parameters signify performance of the proposed algorithm which can be further utilized for Park and Ang damage index calculation. This is otherwise difficult to quantify using other non-destructive or destructive tools. It is the main objective of this study which augments the decision-making process for rehabilitation and retrofitting.

Table 3 Comparison of actual and estimated EDPs

δm_m^{ac} (mm)	δm_m^{est} (mm)	$\epsilon_{\delta m}$ (%)	$\int dE_h^{ac}$ (kNmm)	$\int dE_h^{est}$ (kNmm)	ϵ_{E_h} (%)
5.2725	5.2751	0.0493	1.6583×10^5	1.6473×10^5	0.6632

*superscripts *ac* and *est* stand for actual and estimated cases

5.2 Full scale bridge pier test

Once the performance of the proposed algorithm is established using simulated Bouc-Wen hysteretic response, it is further used for damage estimation of a full-scale structure under earthquake excitation. In this case, experimental data of a circular reinforced concrete bridge pier under uniaxial seismic excitation is used, which was tested NEES-UCSD large High-Performance Outdoor Shake Table as shown in Fig.6a. The full-scale RC bridge pier has a diameter of 1.22 m and its height is 7.32 m. To simulate the mass of the superstructure, a concrete block weighing 2245 kN is placed on top of the column. The PEER report no. 2015/02 Schoettler *et al.* (2012) has all the necessary information regarding the instrumentation and the loading protocol. The structure was subjected to different earthquake ground excitations in succession which correspond to the different intensity levels.

In this study, the EQ5-EQ8 sequences are selected for damage estimation purposes. The details of these ground motions are presented in Table 4. The sensor placements are shown in Fig. 6(b) in which the naming of the sensors are kept consistent with the original data file available in the DESIGNSAFE-CI platform Rathje *et al.* (2017). To accommodate the available measurements of the test specimen, the column has been modelled as a 2-DOF system under ground excitation. Points B and C in Fig. 6(b) correspond the DOF x_1 and x_2 (as in Fig. 2) in equivalent sense. As observed during the experiment, non-linearity is concentrated at the base of the column and the plastic hinge is modelled there by Bouc-Wen hysteresis. Since the geometry and material properties of the specimen are available, they are considered for mass estimation of the structure. Due to the minimal axial load ratio (i.e., 5.3%), stiffness degradation was very unlikely to occur during the experiment.

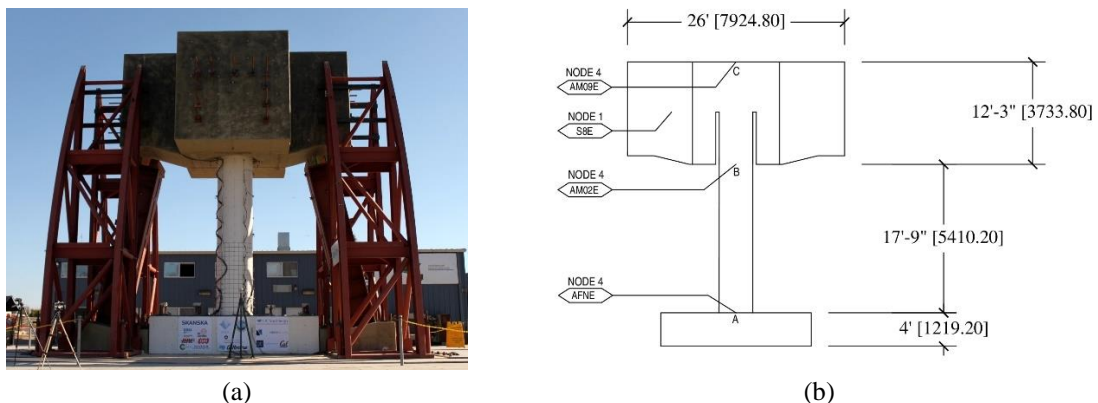


Fig. 6 Full scale test of bridge pier; (a) Experimental setup (Courtesy: DESIGNSAFE-CI) and (b) Schematic diagram of test setup and sensor placement

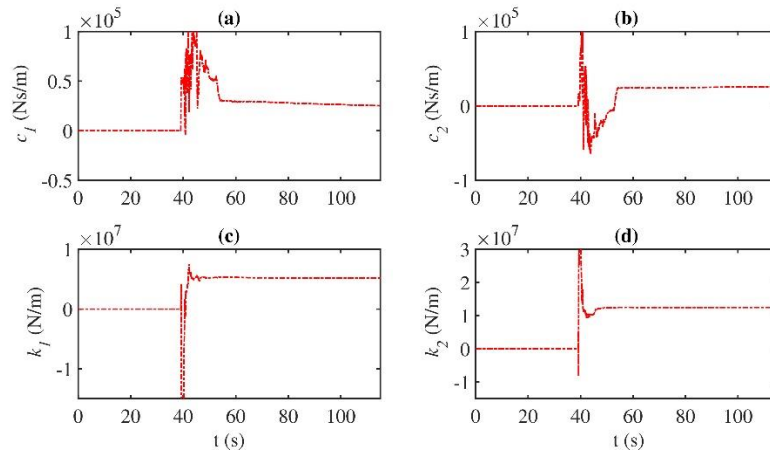


Fig. 7 Identified stiffness and damping co-efficients of bridge pier; (a) damping coefficient c_1 , (b) damping coefficient c_2 , (c) stiffness k_1 & (d) stiffness k_2

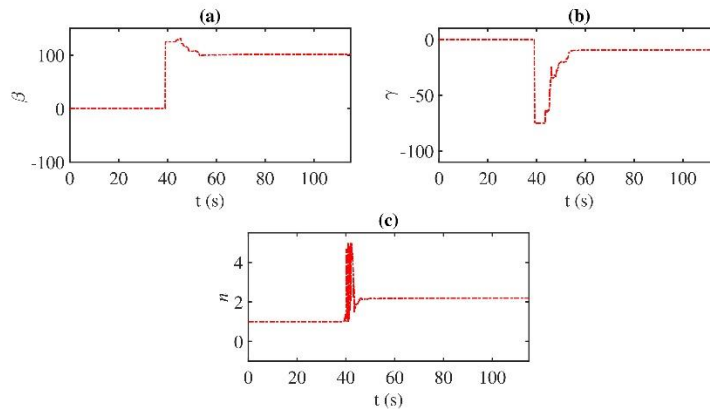


Fig. 8 Identified Bouc-Wen parameter of bridge pier; (a) parameter β , (b) parameter γ and (c) parameter n

Table 4 Ground motion details

Tests	Earthquake	Year	Station	Moment Magnitude	Scale	PGA
EQ5	Kobe	1995	Takatori	6.9	-0.8	-0.533
EQ6	Loma Prieta	1989	LGPC	6.9	1	-0.512
EQ7	Kobe	1995	Takatori	6.9	-1.2	0.646
EQ8	Kobe	1995	Takatori	6.9	1	-0.829

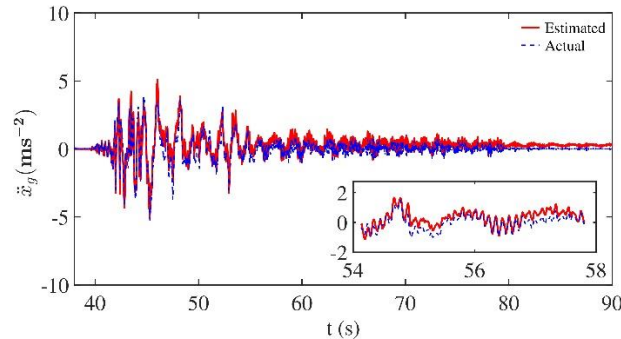


Fig. 9 Comparison of input for bridge pier test

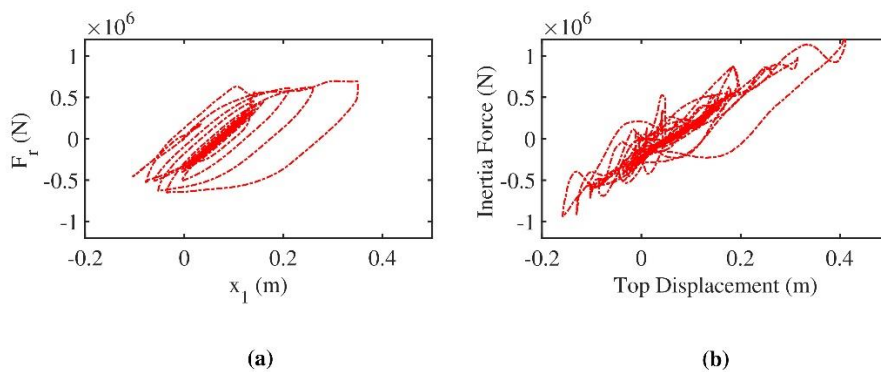


Fig. 10 Comparison of hysteresis plot for EQ5 case; (a) using proposed method and (b) as estimated by Shan *et al.* (2019)

Hence, a non-degrading classical Bouc-Wen model is adopted in this case. The equation of motion of this system can be expressed by Eq. (44) along with $z(t)$ in Eq. (1(b)) as the hysteretic displacement.

Similar to the previous example, the extended state vector is formed as in Eq. (18), where, $\mathbf{\Lambda} = \{x_1 \ x_2 \ \dot{x}_1 \ \dot{x}_2 \ z\}$, $\mathbf{\Theta} = \{\alpha \ n\}$ and $\mathbf{w} = [k_1 \ k_2 \ c_1 \ c_2]$. The parameter bound for $\mathbf{\Theta}$ and the BIBO property remain same as in the example 1. The measurement vector is composed of recorded accelerations \ddot{x}_1 and \ddot{x}_2 (i.e., AM02E and AM09E readings) and displacement x_2 (i.e., S8E readings), which is expressed as $\{x_1 \ \ddot{x}_1 \ \ddot{x}_2\}$. The Gaussian noise associated with the measurement is assumed to have zero mean, whose covariance matrix is \mathbf{R}_k has diagonal elements only. Using these inputs, the stiffness and damping coefficients as well as the Bouc-Wen parameters converged at a time around 50s as shown in Figs. 7 and 8 owing to the satisfactory performance of the proposed algorithm. Besides system parameters, input ground motion also shows satisfactory

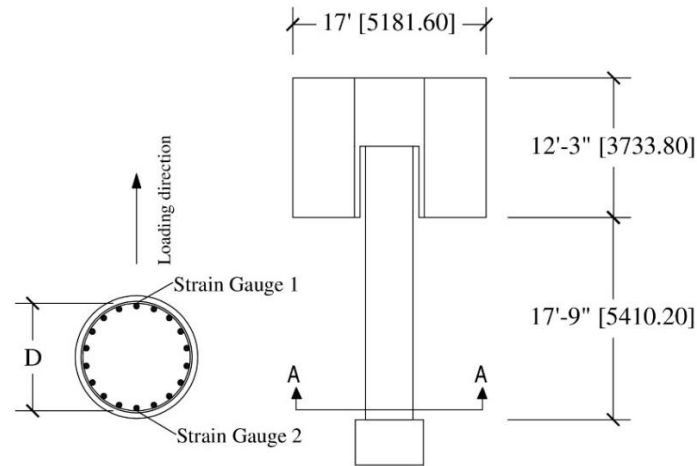


Fig. 11 Schematic diagram of strain gauge positions

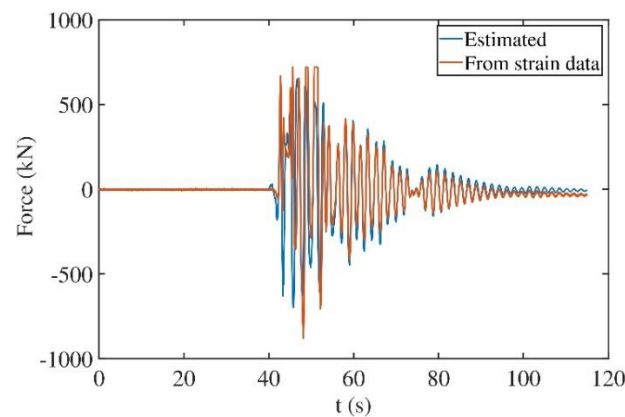


Fig. 12 Estimated force from strain data for EQ5 case

matching with the measured shake table response at a point A as shown in Fig. 9, which indicates that the estimated parameters have reasonable accuracy. One of the major advantages of the proposed method is the ability to estimate the restoring force acting on the structure which is otherwise difficult to quantify. In absence of restoring force measurement, designers often assume the total inertia force as the base shear acting on the structure. A similar practice was observed in Shan *et al.* (2019) for the same EQ5 sequence used in this paper. The comparison between the proposed method and the hysteresis plot obtained by following the assumption in Shan *et al.* (2019) is shown in Fig.10. A distinct difference between the nature of hysteresis plots is observed in both of these approaches. The proposed algorithm can capture the actual nature of the hysteresis plot while the other approach as adopted by Shan *et al.* (2019) fails to do so. The main difference arises due to the contribution of inherent damping of the structure which is balanced by the total inertia force along with the nonlinear spring force and hence, the estimation of the restoring force is incorrect, which leads to the hysteresis plot in the study by Shan *et al.* (2019).

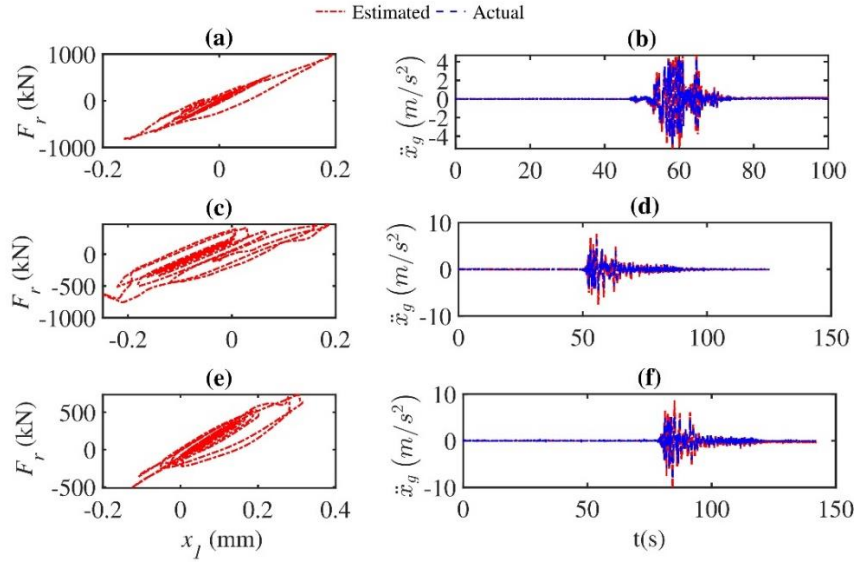


Fig. 13 Estimated hysteresis behaviour and input ground motion for different events; (a) EQ6 hysteresis, (b) EQ6 input ground motion (c) EQ7 hysteresis, (d) EQ7 input ground motion (e) EQ8 hysteresis and (f) EQ8 input ground motion

Table 5 Cumulative estimated damage index for EQ5-EQ8 sequence

Event	F_y (KN)	δ_m (m)	β_d	$\int d E_h$ (kNm)	DI	Remark
EQ5	782	0.35	0.04	6.65E+02	0.69	Spalling of cover concrete
EQ6	782	0.19	0.04	1.04E+02	0.70	Spalling of cover concrete
EQ7	782	0.24	0.04	2.45E+02	0.73	Reinforcement exposed
EQ8	782	0.31	0.04	2.69E+02	0.75	Cracks in core-concrete

5.2.1 Validation of proposed method with strain measurement

To validate the proposed algorithm further, strain data acquired during the experiment has been considered. The strain measurements are obtained from the gauges installed on the longitudinal reinforcements situated on the opposite sides of the specimen in a plane parallel to the loading direction. The strain measurements are utilized to obtain the curvature (ϕ_c) of the section from the following expression

$$\phi_c = \frac{\varepsilon_2 - \varepsilon_1}{D} \quad (45)$$

where, ε_1 and ε_2 are the strain measurements obtained at section AA using electrical resistant strain gauges with effective gauge length of 5mm as shown in Fig. 11 from gauge 1 and gauge 2. D is the distance between the gauge mounting points. Further, the obtained curvature time history has been employed to calculate the moment time-history using the monotonic moment-curvature relationship.

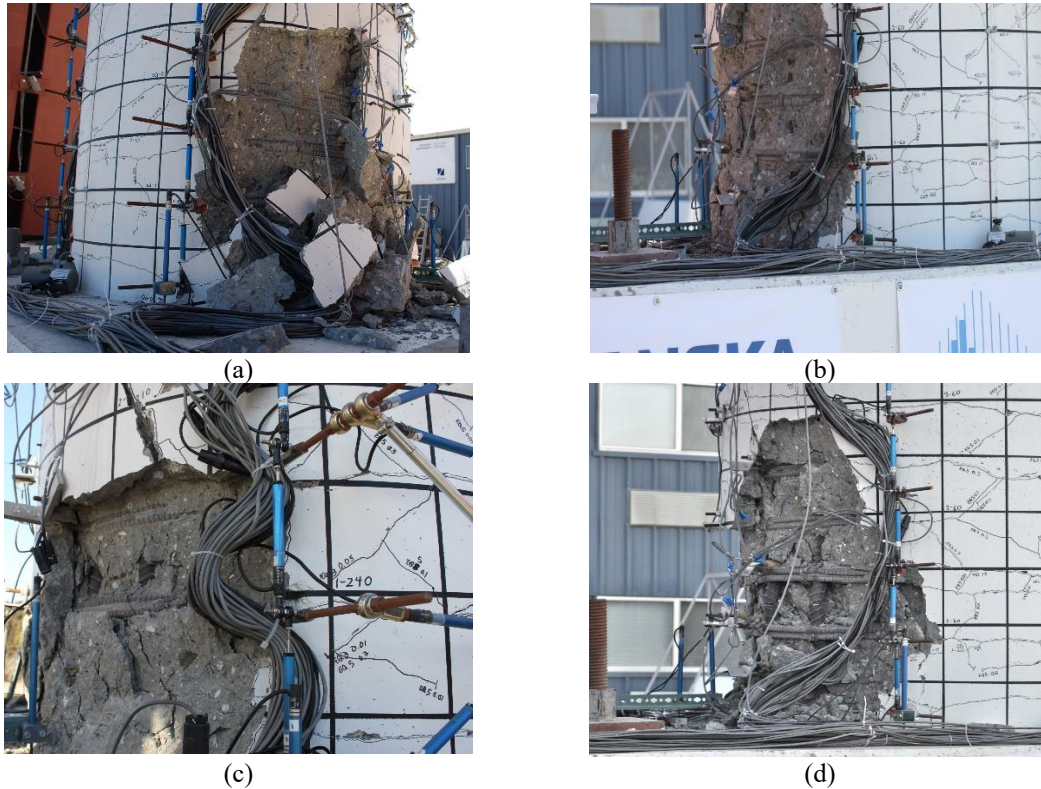


Fig. 14 Observed damage during shake table experiment (a) EQ5 (b) EQ6 (c) EQ7 and (d) EQ8

It is assumed that the moment at section AA is due to the response of the SDOF system whose mass is lumped at the top. By this assumption, the force experienced at section AA is calculated from moment time-history using the force-moment relationship of a cantilever column. The comparison of estimated restoring force by the proposed method and the same obtained from the strain measurements is shown in Fig. 12. Although they differ marginally for the initial few seconds, an excellent matching of these is observed beyond 50s. During the initial few seconds, the structure experiences very high inelastic demand which compel the sectional curvature demand to go beyond its elastic range and hence, the linear relationship fails to capture the actual restoring force accurately. However, as long as the sectional curvature is within elastic range the (i.e., beyond 50s) a satisfactory match in terms of amplitude and frequency is observed between them.

5.2.2 Park and Ang damage index estimation

In this subsection, the Park and Ang damage index is estimated for the EQ5-EQ8 earthquake sequences as shown in Table 5. The capacity related parameters i.e. yield force F_y , yield displacement δ_y and ultimate displacement δ_u are taken from the PEER report no. 2015/02 Schoettler *et al.* (2012), which are given as $F_y = 781.8$ (kN), $\delta_y = 88$ (mm) and $\delta_u = 506$ (mm). To calculate the parameter β_d , that involved in Park and Ang DI, the following equation provided by Park and Ang (1985) is used here

$$\beta_d = \left(-0.447 + 0.073 \frac{l}{d} + 0.24n_o + 0.314p_t \right) \times 0.7^{\rho_w} \quad (46)$$

where, $\frac{l}{d}$ is the shear span ratio, n_o is the normalized axial stress, p_t is the longitudinal steel ratio, and ρ_w is the confinement ratio. The demand related parameters used in this process are obtained from the proposed method for three ground motion sequences (i.e., EQ6-EQ8), which are shown in Fig. 13. The engineering damage parameters are obtained using the proposed algorithm, which are further utilized for damage index estimation as shown in Table 5. During the EQ5 event, spalling of cover concrete was observed, however, no damage in core concrete had occurred during the experiment. In the next two events (i.e., EQ6 and EQ7), spalling of cover concrete intensified and longitudinal reinforcements were exposed to the environment. At the end of EQ8 event, some damage took place at the core concrete along with the loss of integrity of the confining reinforcements. These gradual increase in damage state is also reflected in the commutative damage index as shown in Table 5. Here, EQ5 shows the least value of damage while EQ8 corresponds to the highest level, which is consistent with the observed damage state as shown in Fig. 14.

5. Conclusions

In this paper, the constrained minimum variance unbiased estimator is used to quantify the in-situ damage in a RC bridge pier from the recorded measurements. The hysteretic behaviour of the concrete is characterized by the advanced version of Bouc-Wen model incorporating both degradation and pinching effects. To maintain stability and convergence, suitable constraint conditions are enforced to the original generalized minimum variance unbiased estimator using unscented sigma points. The overall conclusions from the numerical results presented in the previous section are as follows -

- The effectiveness of the algorithm is first demonstrated with the help of a simulated case having degradation and pinching effects. The results show excellent performance of the algorithm to estimate the engineering demand parameters with a high level of accuracy.
- This is followed by a full-scale shake table tests of RC bridge pier to quantify the restoring force as well as the input ground motion. The estimated restoring force obtained from the proposed algorithm provides satisfactory matching with the force value obtained from the measured strain data.
- The cumulative damage index obtained for the bridge pier establishes a good correlation with the observed damage state, which can be extremely useful in decision making for rehabilitation /retrofitting of the structure. Thus, the major contribution of this study is to facilitate decision making process based on the in-situ condition assessment after any seismic event.
- Besides the above observation, another major advantage of the proposed inverse algorithm is that it can identify the input to the system satisfactorily. This is extremely helpful for structures having no dedicated sensors for earthquake measurement. The identified input motion is the best possible candidate for demand estimation and for the performance evaluation of the rehabilitated structure.

Acknowledgments

Authors wish to acknowledge Dr. Matthew Schoettler and Professor Jose Restrepo for sharing the full-scale bridge pier test data in the public domain (i.e. DESIGNSAFE-CI platform).

References

- Bouc, R. (1967), "Forced vibrations of mechanical systems with hysteresis", *Proceedings of the 4th Conference on Nonlinear Oscillations*, Prague.
- Baber, T.T. and Noori, M.N. (1985), "Random vibration of degrading, pinching systems", *J. Eng. Mech.*, **111**(8), 1010-1026.
- Bisht, S.S. and Singh, M.P. (2014), "An adaptive unscented Kalman filter for tracking sudden stiffness changes", *Mech. Syst. Signal Pr.*, **49**(1), 181-195.
- Calabrese, A., Strano, S. and Terzo, M. (2018), "Adaptive constrained unscented kalman filtering for real-time nonlinear structural system identification", *Struct. Control Health Monit.*, **25**(2), e2084.
- Chang, C.M., Strano, S. and Terzo, M. (2016), "Modelling of hysteresis in vibration control systems by means of the bouc-wen model", *Shock and Vibration*.
- Chang, G. and Mander, J.B. (1994), "Seismic energy based fatigue damage analysis of bridge columns: Part I-Evaluation of seismic capacity", National Center for Earthquake Engineering Research Buffalo, New York.
- Chatzi, E.N., Smyth, A.W. and Masri, S.F. (2010), "Experimental application of on-line parametric identification for nonlinear hysteretic systems with model uncertainty", *Struct. Saf.*, **32**(5), 326-337.
- Gaviria, C.A. and Montejo, L.A. (2019), "Monitoring physical and dynamic properties of reinforced concrete structures during seismic excitations", *Constr. Build. Mater.*, **196**, 43-53.
- Ghosh, S., Datta, D. and Katakdhond, A.A. (2011), "Estimation of the park-ang damage index for planar multi-storey frames using equivalent single-degree systems", *Eng. Struct.*, **33**(9), 2509-2524.
- Gillijns, S. and De Moor, B. (2007a), "Unbiased minimum-variance input and state estimation for linear discrete-time systems", *Automatica*, **43**(1), 111-116.
- Gillijns, S. and De Moor, B. (2007b), "Unbiased minimum-variance input and state estimation for linear discrete-time systems with direct feedthrough", *Automatica*, **43**(5), 934-937.
- Gucunski, N., Kee, S., La, H., Basily, B. and Maher, A. (2015), "Delamination and concrete quality assessment of concrete bridge decks using a fully autonomous robot platform", *Struct. Monit. Maint.*, **2**(1), 19-34.
- Hernandez, E.M. and May, G. (2012), "Dissipated energy ratio as a feature for earthquake-induced damage detection of instrumented structures", *J. Eng. Mech.*, **139**(11), 1521-1529.
- Ibarra, L.F., Medina, R.A. and Krawinkler, H. (2005), "Hysteretic models that incorporate strength and stiffness deterioration", *Earthq. Eng. Struct. D.*, **34**(12), 1489-1511.
- Ikhoulane, F. and Rodellar, J. (2005), "On the hysteretic bouc-wen model", *Nonlinear Dynam.*, **42**(1), 63-78.
- Ikhoulane, F., Mañosa, V. and Rodellar, J. (2007), "Dynamic properties of the hysteretic bouc-wen model", *Systems Control Letters*, **56**(3), 197-205.
- Julier, S.J. and Uhlmann, J.K. (1997), "New extension of the kalman filter to nonlinear systems", *Signal processing, sensor fusion, and target recognition VI*, **3068**, 182-193.
- Kandepu, R., Imsland, L. and Foss, B.A. (2008), "Constrained state estimation using the unscented kalman filter", *Proceedings of the 2008 16th Mediterranean Conference on Control and Automation*, IEEE.
- Lin, S.W., Yi, T.H., Li, H.N. and Ren, L. (2017), "Damage detection in the cable structures of a bridge using the virtual distortion method", *J. Bridge Eng.*, **22**(8), 04017039.
- Li, H.N., Qu, C., Huo, L. and Nagarajaiah, S. (2016), "Equivalent bilinear elastic single degree of freedom system of multi-degree of freedom structure with negative stiffness", *J. Sound Vib.*, **365**, 1-14.
- Mandela, R., Kuppuraj, V., Rengaswamy, R. and Narasimhan, S. (2012), "Constrained unscented recursive estimator for nonlinear dynamic systems", *J. Process Control*, **22**(4), 718-728.
- Nair, A., Cai, C., Pan, F. and Kong, X. (2014), "Acoustic emission monitoring of damage progression in CFRP

- retrofitted rc beams”, *Struct. Monit. Maint.*, **1**(1), 111-130.
- Nithin, V.L. (2019), “Stochastic simulation of main shock-aftershock sequences and their use in damage-based seismic design of reinforced concrete structures”, Ph.D. Dissertation; Indian Institute of Technology Guwahati, India.
- Park, Y.J. and Ang, A.H.S. (1985), “Mechanistic seismic damage model for reinforced concrete”, *J. Struct. Eng.*, **111**(4), 722–739.
- Providakis, C., Tsistrakis, S., Voutetaki, M., Tsompanakis, Y., Stavroulaki, M., Agadakos, J., Kampianakis, E. and Pentos, G. (2015), “A new damage identification approach based on impedance-type measurements and 2d error statistics”, *Struct. Monit. Maint.*, **2**(4), 319-338.
- Qu, C.X., Mei, D.P., Yi, T.H. and Li, H.N. (2017), “Spurious mode distinguish by modal response contribution index in eigensystem realization algorithm”, *Struct. Des. Tall Spec. Build.*, **27**(12), e1491.
- Qu, C.X., Yi, T.H., Li, H.N. and Chen, B. (2018a), “Closely spaced modes identification through modified frequency domain decomposition”, *Measurement*, **128**, 388-392.
- Qu, C.X., Yi, T.H., Zhou, Y.Z., Li, H.N. and Zhang, Y.F. (2018b), “Frequency identification of practical bridges through higher-order spectrum”, *J. Aerosp. Eng.*, **31**(3), 04018018.
- Qu, C.X., Yi, T.H. and Li, H.N. (2019). “Mode identification by eigensystem realization algorithm through virtual frequency response function”, *Struct. Control Health Monit.*, **26**(10), e2429.
- Rathje, E.M., Dawson, C., Padgett, J.E., Pinelli, J.P., Stanzione, D., Adair, A., Arduino, P., Brandenberg, S. J., Cockerill, T. and Dey, C. (2017), “Designsafe: new cyberinfrastructure for natural hazards engineering”, *Natural Hazards Review*, **18**(3), 06017001.
- Schoettler, M.J., Restrepo, J., Guerrini, G., Duck, D.E. and Carrea, F. (2012), “A full-scale, single-column bridge bent tested by shake-table excitation”, *Center for Civil Engineering Earthquake Research, Department of Civil Engineering, University of Nevada*.
- Shan, J., Ouyang, Y., Zhang, H. and Shi, W. (2019), “Model-reference damage tracking and evaluation of hysteretic structures with test validation”, *Mech. Syst. Signal Pr.*, **118**, 443-460.
- Sengupta, P. and Li, B. (2013), “Modified Bouc–Wen model for hysteresis behavior of RC beam–column joints with limited transverse reinforcement”, *Eng. Struct.*, **46**, 392-406.
- Sengupta, P. and Li, B. (2017), “Hysteresis modeling of reinforced concrete structures: state of the art”, *ACI Struct. J.*, **114** (1).
- Song, W. and Dyke, S. (2013), “Real-time dynamic model updating of a hysteretic structural system”, *J. Struct. Eng.*, **140**(3), 04013082.
- Song, W. (2018), “Generalized minimum variance unbiased joint input-state estimation and its unscented scheme for dynamic systems with direct feedthrough”, *Mech. Syst. Signal Pr.*, **99**, 886-920.
- Todorovska, Maria I. and Trifunac, Mihailo D. (2007), “Earthquake damage detection in the Imperial County Services Building I: The data and time–frequency analysis”, *Soil Dynam. Earthq. Eng.*, **27**, 564-576.
- Wei, A., Wang, Y. and Tan, M.Y. (2015), “Monitoring corrosion of reinforced concrete beams in a chloride containing environment under different loading levels”, *Struct. Monit. Maint.*, **2**(3), 253-267.
- Wen, Y.K. (1976), “Method for random vibration of hysteretic systems”, *J. Eng. Mech. Division*, **102**(2), 249-263.
- Williams, M.S. and Sexsmith, R.G. (1995), “Seismic damage indices for concrete structures: a state-of-the-art review”, *Earthq. spectra*, **11**(2), 319-349.
- Wu, M. and Smyth, A.W. (2007), “Application of the unscented kalman filter for real-time nonlinear structural system identification”, *Struct. Control Health Monit.*, **14**(7), 971-990.
- Tzoura, E.A., Triantafillou, T.C., Providakis, C., Tsantilis, A., Papanicolaou, C.G. and Karabalis, D. (2015), “Damage detection of reinforced concrete columns retrofitted with FRP jackets by using PZT sensors”, *Struct. Monit. Maint.*, **2**, 165-180.
- Yang, Y. and Ma, F. (2003), “Constrained kalman filter for nonlinear structural identification”, *Modal Anal.*, **9**(12), 1343-1357.
- Yi, T.H., Yao, X.J., Qu, C.X. and Li, H.N. (2019), “Clustering number determination for sparse component analysis during output-only modal identification”, *J. Eng. Mech.*, **145**(1), 04018122.
- Zahrah, T.F. and Hall, W.J. (1984), “Earthquake energy absorption in sdof structures”, *J. Struct. Eng.*, **110**(8),

1757-1772.

Zhang, C., Huang, J.Z., Song, G.Q., Dai, L. and Li, H.K. (2016), "Detection of structural damage via free vibration responses by extended Kalman filter with Tikhonov regularization scheme", *Struct. Monit. Maint.*, **3**(2), 115-127.

JK